Medicinal Chemistry Research (2019) 28:1246–1263
https://doi.org/10.1007/s00044-019-02370-0

MEDICINAL CHEMISTRY RESEARCH

ORIGINAL RESEARCH

3D-QSAR, molecular docking, and new compound design of pyrimidine derivatives as Src small molecule inhibitors

Jun-wei Wang[1,2] · Ya-ting Deng[1,2] · Han Chu[1,2] · Juan Wang[1,2] · Yong Hu[1,2] · Zhi-hua Lin[1,2]

Received: 9 February 2019 / Accepted: 22 May 2019 / Published online: 5 June 2019

Abstract

Non-receptor tyromethod, The sine kinase Src is one of the important molecular targets for potential triple-negative breast cancer (TNBC). In this study, the structure and acitivity relationship of 51 Src small molecule inhibitors with potential pyrimidine derivatives was explored. On the basis of ligand composite, the relationsConducted a phase hip between molecular structure and inhibitory activity of MDA-MB-231/435 TNBC cell lines was studied by using comparative molecular field analysis (CoMFA), comparative molecular similarity indices analysis fields (CoMSIA), and Topomer CoMFA (T-COMFA) methods, and thereby two sets of three-dimensional quantitative structure–activity relationship models were established to analyze the molecular structure and anti-TNBC activity. The results indicated that the q^2 of CoMFA, CoMSIA, and Topomer CoMFA models was 0.698/0.719, 0.73/0.684, 0.674/0.683, and r^2 was 0.994/0.991, 0.991/0.985, 0.946/0.959, respectively. Moreover, the three-dimensional equipotential map also revealed the relationship between structural characteristics and inhibitory activity, and molecular docking was investigated by Surflex-dock. The data proved that this model had good predictive ability and can further guide the design and modification of 3- (phenylethynyl) −1 hydropyrazolyl [3anilo-d] pyrimidine-4-amine derivatives inhibitors. According to the three-dimensional quantitative structure–activity relationship model of two TNBC cell lines of MDA-MB-231/435, 13 and 11 compounds were designed respectively, and the predicted activity values showed effective inhibition of SRC.

Keywords Triple-negative breast cancer · Src · 3D-QSAR · Molecular docking · Design

Introduction

Breast cancer is one of the most common cancers among women. As a heterogeneous disease, there are multiple subtypes that have different molecular phenotypes, clinical features, and responses to treatment (Park et al. 2015). The classical immunopathological classification is based on the expression of estrogen receptor alpha (ERα), progesterone receptor (PR), and human epidermal growth factor receptor-2 (HER-2). Triple-negative breast cancer (TNBC) refers to breast cancer with negative ERα and PR expression and negative HER-2/Neu receptor overexpression, which accounts for 10.0–20.8% of all breast cancer pathological types (Bianchini et al. 2016). The average age of onset of TNBC is relatively small, the degree of malignancy is high, progress is relatively fast, and the rate of local recurrence and distant metastasis is high. Only 30% of patients can increase the 5-year survival rate and lack specific molecular targets (Dent et al. 2007). In recent years, identification of gene mutations and signaling pathways has identified some potential molecular targets, some of which have been used to develop targeted therapies. Although many targeted therapies for TNBC have been developed, chemotherapy remains the only clinical option for TNBC, of which Src is one of the most promising targets (Liedtke and Rody 2015).

The non-receptor tyrosine kinase Src is a regulatory protein (Kim et al. 2009), Src is the first discovered oncogene (Rexer and Arteaga 2012), In cell differentiation, movement, invasion, proliferation, and other life activities have an important regulatory role, participate in, and promote the progress and metastasis of a variety of malignant

The first author: Wang Jun-wei, E-mail:694270113@qq.com

✉ Zhi-hua Lin
zhlin@cqut.edu.cn

[1] Department of Pharmacy and Bioengineering, Chongqing University of Technology, Chongqing 400054, China

[2] Key Laboratory of Screening and activity evaluation of targeted drugs, Chongqing 400054, China

tumors. It has been shown to have an important role in the proliferation, migration, and invasion of breast cancer cell lines (Zhang et al. 2013; Shields et al. 2013). In addition, abnormal activation or expansion of Src was also detected in the tumor tissue of TNBC patients (Tryfonopoulos et al. 2011). Recent studies have shown that Src is overexpressed and activated in malignant tumors such as breast cancer, gastric cancer, and colon cancer (Mayer and Krop 2010). In breast cancer, studies have shown that Src is significantly associated with bone metastases and lung metastases in breast cancer (Myoui et al. 2003). Most importantly, Src has recently been identified as a therapeutic target for basic breast cancer including TNBC subtypes (Lehmann 2011). Currently, there are several Src inhibitors in clinical trials (Tarpley et al. 2014), its target patients are mainly advanced breast cancer patients. However, dasatinib is the only src inhibitor that treats TNBC in clinical trials (Finn et al. 2011).

On 28 June 2006, Dasatinib (BMS-354825) was approved by the Food and Drug Administration (FDA) for the treatment of acute lymphoblastic leukemia (ALL) and chronic myelogenous leukemia (CML) (Pathak et al. 2015). For the treatment, previously used cancer drugs include imatinib-resistant or intolerant drugs (Seggewiss et al. 2008). Dasatinib is an orally active ATP-competitive small-molecule kinase inhibitor that effectively inhibits Abl kinase, Src family kinases, and other kinases. From in vitro biochemical kinase analysis data, this drug also effectively inhibits a variety of other kinases, including c-Kit, PDGFR, and kinases. In addition to its activity on leukemia cells, dasatinib has also been shown to inhibit cell proliferation in many different types of tumor cell lines, including basal TNBC (Davis et al. 2014), gastric cancer (Okamoto et al. 2010), pancreatic cancer (Pan et al. 2015), ovarian cancer (Haltia et al. 2017), prostate cancer (Massard et al. 2017), and lung cancer (Montero et al. 2011). The activity of these solid tumors is attributed to the inhibition of Src family kinases. Dasatinib inhibits tumor growth and metastasis in mouse models of prostate and pancreatic cancer (Park et al. 2008). Therefore, a large number of clinical trials are underway, in which dasatinib is being evaluated as a monotherapy or in combination with other cancer drugs for a variety of types of cancer. The clinical TNBC model also showed that dasatinib showed synergistic or additive activity with chemotherapy, suggesting that dasatinib may have clinical benefit in TNBC (Pichot et al. 2009). Finn et al. (2011) conducted a phase II clinical trial to evaluate the efficacy and safety of dasatinib monotherapy in patients with advanced TNBC, but the results showed that the rate of disease control achieved by dasatinib monotherapy was 9.3%. It shows that the efficacy of dasatinib monotherapy in TNBC patients is limited. The fact that dasatinib has a subnanomolar inhibitory activity on Src (IC50 = 0.0003 μm) suggests that it is impractical to further enhance the anti-TNBC activity of the compound by increasing the Src inhibition potency alone (Das et al. 2006). Owing to the high heterogeneity of TNBC, a multi-target strategy may be a better choice for enhancing the anti-TNBC activity of Src inhibitors. Therefore, in recent years, Zhang et al. (2016) developed a multi-enzyme inhibitor of 3-(phenylethynyl)-1H-pyrazolo[3,4-d]pyrimidin-4-amine derivatives. This article is from the study by Zhang et al. (2016). In the literature, three-dimensional quantitative structure–activity relationship (3D-QSAR) studies were conducted on a series of novel compounds. Among them, No. 43 molecule has the highest activity value among the experimental values in the original text. In this paper, the 3D-QSAR model was successfully established after the three-dimensional structure–activity analysis of the compound, in order to provide feasible suggestions for the future synthesis of Src inhibitors.

3D-QSAR is a statistical analysis tool and theoretical calculation to study the quantitative relationship between the three-dimensional molecular structure of a series of compounds and their biological activity. It is an important theory and common method in drug research (Zhang et al. 2011). In this paper, 51 Src inhibitors were selected and 3D-QSAR models were established for two TNBC cell lines, MDA-MB-231/435, using CoMFA, comparative molecular similarity indices analysis fields (CoMSIA), and Topomer CoMFA, which are common in 3D-QSAR. The results show that the two models built have good predictability and stability. The analysis results of the three-dimensional equipotential map reveal (Morales-Bayuelo et al. 2010) a more comprehensive and intuitive relationship between the physicochemical properties of Src inhibitors and their biological activities, providing a reliable statistical model for the design, screening, and activity prediction of new compounds.

Materials and methods

Data sources and molecular structure optimization

The 51 pyrimidine derivative compounds selected in this article are from the literature (Zhang et al. 2016). Using chembiodraw ultra 14.0 software to draw the Src inhibitor molecules that were selected from the literature for activity measured by the same method. The public skeleton is shown in Fig. 1. The activity values, predicted activity values, and molecular structures of molecular experiments are shown in Table 1. The activity value of a molecule is the conversion of the IC50 of the molecule to pIC50 (–lgIC50). The MDA-MB-231 and MDA-MB-435 were, respectively, constructed as a 3D-QSAR model. In the MDA-MB-231 QSAR model, 33

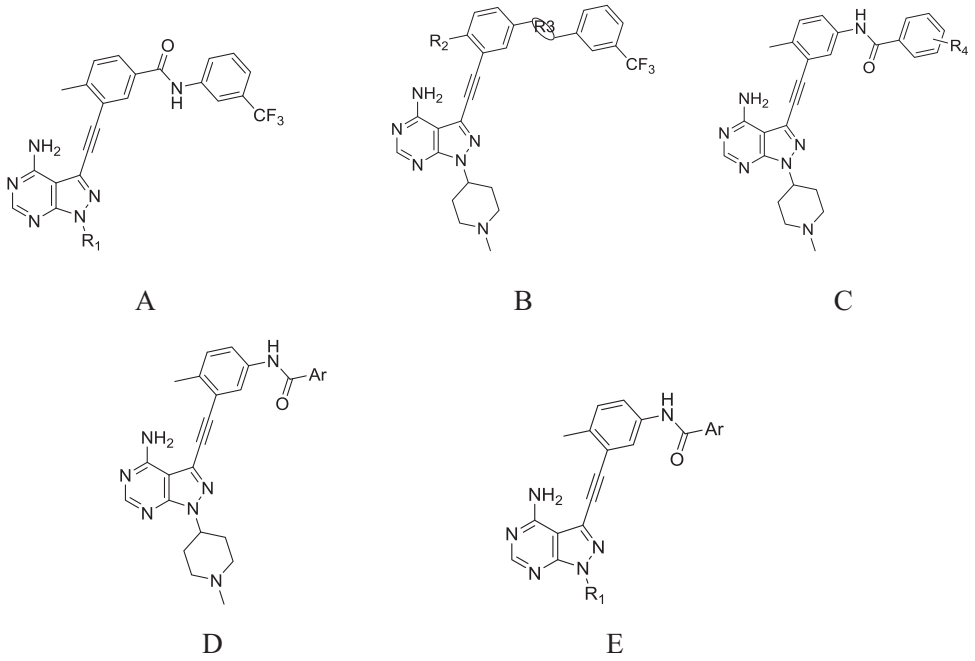

Fig. 1 Pyrimidine derivative structure skeleton. **a** molecules 1–5, **b** molecules 6–13, **c** molecules 14–30, **d** molecules 31–36, **e** molecules 37–51

compounds were randomly selected as the training set and 12 compounds were the test set. In the MDA-MB-435 QSAR model, 32 compounds were randomly selected as the training set and 12 compounds were the test set. The molecules were constructed and optimized using Tripos SybylX2.1, Tripos force field, Gasteiger-Huckel charge, Powell energy gradient method, 10,000 times optimization, and energy convergence difference 0.005 kcal/mol. Other values are default, and molecular mechanics optimization is performed on the compounds to obtain the lowest energy conformation of the molecule and the lowest energy conformation is the active conformation. The half inhibitory concentration IC50 of the 3-(phenylethynyl)-1hydro-pyrazolo[3,4-d]pyrimidin-4-amine derivative Src inhibitor was converted into pIC50 (negative logarithm of IC50) as the dependent variable for the study afterwards. In the Aligen database module, the optimized maximum activity of No. 43 molecule was used as a template for superposition. The degree of molecule overlap was related to the prediction ability of the model. The overlap was shown in Fig. 2. All molecules can be superimposed together.

Establishment of 3D-QSAR model

In this article, 3D-QSAR studies of compounds were performed using the three most classical methods in SYBYL—CoMFA, CoMSIA, and Topomer CoMFA. In SYBYL2.1, using the Tripos force field, the superimposed training set molecules were placed in a 2 Å step size grid, with a positively charged sp^3 hybrid carbon atom as the stereo probe, with a positive Charged hydrogen atoms act as electrostatic probes, comparative molecular field analysis (CoMFA) is one of the most representative methods of the 3D-QSAR model (Kakarla et al. 2016), which requires spatial superposition of ligand conformations, with stereo and electrostatic fields as independent variables, and negative logarithm of molecular agonistic activity as dependent variables, using partial least squares (PLS) modeling, and PLS is an extension of multiple regression analysis (Bush and Nachbar 1993).

Leave-one-out is used for cross-validation (Taha et al. 2014). After the optimal cross-validation coefficient q^2 is obtained, the best principal component number (n) is determined. Then based on the best principal component number (n), non-cross-validation was performed to obtain the correlation coefficient r^2, standard deviation (SEE), F value and contribution value of each position. The CoMFA model was obtained. The test set activity was predicted using the above construction model. The CoMSIA is an extension of CoMFA (Sharma et al. 2016), Compared with CoMFA, there is no need to define the cutoff value of energy, so that the equipotential map contributed by different fields can be interpreted more intuitively. In the study, in addition to the introduction of stereo and electrostatic fields, hydrophobic, hydrogen bond acceptor, and hydrogen bond donor fields were introduced to provide a better explanation of the relationship between molecular structure and activity. The general conditions that a 3D-QSAR model with more reliable prediction capability must satisfy are: $q^2 > 0.5$, $r^2 > 0.9$, the F value should be as large as possible, and the SEE value should be as small as possible (Wendt and Cramer 2014).

Table 1 Structure and activity data of 51 compounds

structure			MDA-MB-231				MDA-MB-435			
NO.	R1	PIC50	predicted value			PIC50	predicted value			
			CoMFA	CoMSIA	TCOMFA		CoMFA	CoMSIA	TCOMFA	
1[1,2]	-	7.959	7.914	7.942	8.04	8.301	8.281	8.312	8.19	
2[1,2]	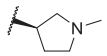	7.886	7.872	7.898	7.90	7.375	7.276	7.342	7.28	
3[2]	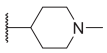					6.770	6.847	6.780	6.54	
4[1,2]	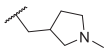	7.387	7.450	7.346	7.43	6.935	6.999	6.951	7.24	
5[1*,2]	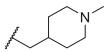	7.155	7.657	7.657	7.58	7.260	7.298	7.269	7.23	
	R2 R3									
6[1,2]	H 	5.773	5.804	5.871	5.79	6.465	6.473	6.502	6.65	
7[1,2]	H 	6.224	6.145	6.203	6.24	6.854	6.711	6.851	6.85	
8[1,2]	H 	5.870	5.789	5.827	5.81	6.254	6.208	6.236	6.27	
9[2]	Me 					7.097	7.228	7.076	6.90	
10[1,2*]	Me 	6.228	6.387	6.342	6.41	7.046	6.851	7.028	6.77	
11[1,2]	Cl 	6.126	6.056	6.076	5.98	6.870	6.795	6.818	6.82	
12[2]	Cl 					6.710	6.706	6.793	6.89	
13[1,2]	Cl 	6.024	6.039	6.032	6.04	6.476	6.538	6.511	6.40	
	R4									
14[1*,2]	4-CF_3	6.069	6.633	6.686	6.22	5.289	5.269	5.323	5.20	
15[1,2]	3-OMe	6.996	7.068	6.983	6.97	6.545	6.773	6.716	6.82	
16[1,2]	4-OMe	5.867	5.829	5.852	5.78	5.051	5.053	5.043	5.03	
17[2]	3-Cl					6.135	6.109	5.959	6.08	
18[1,2]	3-F	6.090	6.127	6.296	6.14	5.685	5.750	6.018	5.71	
19[1,2]	3-OCF_3	7.125	7.069	7.002	6.97	7.032	6.801	6.764	6.82	
20[1*,2]	3-Me	6.876	6.570	6.477	6.43	6.375	6.329	6.366	6.37	
21[1,2]	3-tBu	7.229	7.189	7.218	7.27	7.699	7.739	7.786	7.81	
22[1,2*]	2-F-3-CF_3	6.529	6.680	6.497	6.53	6.564	7.085	6.936	6.76	
23[2]	3-CF_3-4-F					6.207	6.200	6.163	6.45	
24[1,2]	3-F-5-CF_3	6.173	6.189	6.192	6.55	5.845	5.855	5.839	5.86	
25[1]	2-F-5-CF_3	6.697	6.645	6.669	6.83					
26[1*,2*]	4-Cl-3-CF_3	7.509	7.238	7.606	6.97	7.569	7.459	7.667	7.27	
27[1]	4-Me-3-CF_3	7.357	7.376	7.378	6.73					
28[1*,2*]	4-OMe-3-CF_3	7.620	7.201	7.463	7.31	6.080	5.557	6.463	6.11	
29[1]	3,5-diCF_3	7.292	7.314	7.252	7.28					
30[2]	2-F-3-Cl-5-CF_3					5.471	5.486	5.481	5.37	

Table 1 (continued)

NO.	structure R1	MDA-MB-231 PIC50	predicted value CoMFA	CoMSIA	TCOMFA	MDA-MB-435 PIC50	predicted value CoMFA	CoMSIA	TCOMFA
	Ar								
31[1,2*]	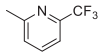	6.293	6.316	6.267	6.47	5.607	5.477	5.476	5.93
32[1]	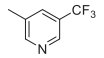	6.777	6.710	6.75	6.70				
33[1]	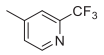	6.547	6.593	6.605	6.78				
34[1,2*]	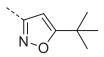	6.726	6.728	6.717	6.75	7.086	6.573	6.810	6.60
35[1*,2*]	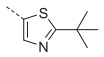	7.108	6.693	6.685	6.63	7.700	7.276	7.347	6.99
36[1*,2*]	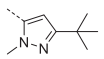	6.489	6.790	6.693	6.66	7.096	6.854	7.064	6.97
	R1 Ar								
37[1,2*]	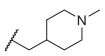	7.959	8.016	7.758	8.01	7.569	7.653	7.388	7.59
38[1,2]	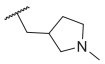	8.046	8.069	8.057	7.86	7.796	7.754	7.792	7.80
39[1*,2]	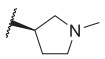	7.854	7.899	7.539	8.32	7.523	7.608	7.511	7.52
40[1,2]	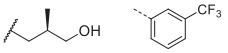	7.770	7.748	7.719	7.76	8.000	8.039	7.994	8.00
41[1,2*]	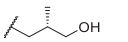	8.000	7.977	8.029	7.76	8.000	8.101	7.631	7.54
42[1*2*]	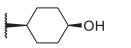	7.866	7.775	7.804	7.92	8.155	7.636	7.802	8.49
43[1,2]	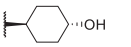	8.046	7.991	8.043	7.92	8.398	8.284	8.364	8.40
44[1*,2]	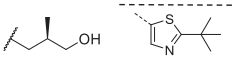	7.469	7.870	8.075	7.15	7.137	7.139	7.151	7.14
45[1,2]	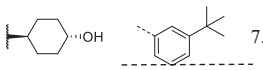	7.523	7.523	7.577	7.43	7.921	7.946	7.958	7.95
46[1,2]	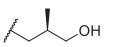	7.319	7.387	7.313	7.59	6.910	6.917	6.948	6.99
47[1*]	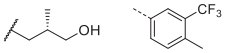	7.367	6.684	7.463	7.59				
48[1,2]	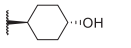	7.523	7.531	7.620	7.75	8.097	8.100	8.120	7.94
49[1,2]	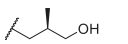	7.638	7.616	7.644	7.63	6.496	6.465	6.464	6.91
50[1*]	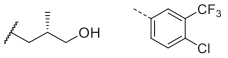	7.770	8.128	7.719	7.63				
51[1,2*]	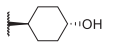	7.796	7.706	7.700	7.78	7.432	7.880	7.745	7.86

1: MDA-MB-231 training set compound; 1*: MDA-MB-231 test set compound; 2: MDA-MB-435 training set compound; 2*: MDA-MB-435 test set compound

Although CoMFA has been widely used in drug design as a relatively successful quantitative structure–activity relationship, it still has many limitations. Its ligand structure must be three-dimensional, and if not, it cannot be reasonably superposed with other molecules. Topomer CoMFA overcomes many of the limitations of CoMFA as a second-generation CoMFA method. Compared with CoMFA, Topomer CoMFA has better reproducibility. In

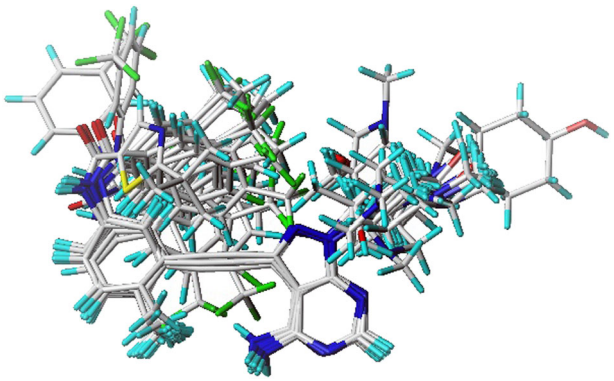

Fig. 2 Alignment of all compounds. The dark blue atom represents nitrogen atom; the light blue atom represents hydrogen atom; the white atom represents carbon atom; the red atom represents oxygen atom; the green atom represents the fluorine atom; the yellow atom represents the sulfur atom

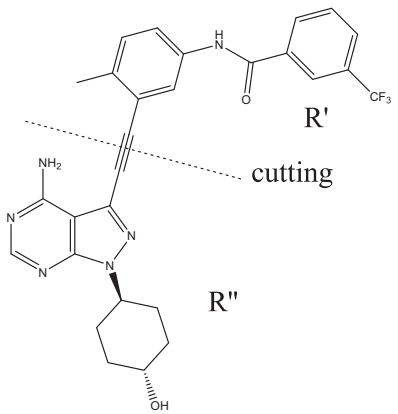

Fig. 3 Molecular cutting diagram

this paper, the inhibitors of 3-(phenylethynyl)-1H-pyrazolo [3,4-d]pyrimidin-4-amine derivatives were analyzed based on the Topomer CoMFA model, The compound with the best activity No. 43 was used as a template, and all the compounds were divided according to the cutting method shown in Fig. 3. The way of dividing the molecules was split in two. All molecules were cleaved in the same manner and the cleaved compound molecules were automatically divided into R', R" groups. The software will use the properties of the stereo and electrostatic fields as independent variables and the pIC50 activity value as the dependent variable. The Topomer CoMFA model will be constructed using PLS. The results of the calculation include the situation of the field around R', R" and their respective contribution to the activity. The test set compounds were cut in the same manner as above and the activity of the test set compounds were predicted using the model constructed above.

Molecular docking

Using the Surflex-Dock plate, Src (PDB:3EL7) was molecularly docked with these 51 molecules, and the binding mode of the receptor and ligand was studied and the results of the 3D-QSAR model were compared. Each small molecule after docking obtained 20 different conformation, choose the best score for the next step to verify.

Summary and discussion

3D-QSAR results and analysis

The statistical results of the 3D-QSAR model obtained by studying the CoMFA and CoMSIA models are shown in Table 2 and Fig. 4. When choosing the model, consider comprehensiveness and reliability, so in MDA-MB-231, choose CoMFA-SE and CoMSIA-SED model. In MDA-MB-435, choose CoMFA-SE and CoMSIA-SEH. In the CoMFA-SE model of MDA-MB-231, the resulting q^2 is 0.698, the best number of principal components is 9, r^2 is 0.994, the SEE is 0.067, and the proportions of the electrostatic field and the stereoscopic field in the model are, respectively, at 24.8% and 75.2%, it can be seen that the stereoscopic field has a greater impact on the model, In the CoMSIA-SED model, the resulting q^2 is 0.755, the best number of principal components is 10, r^2 is 0.993, and the SEE is 0.076. The ratios of stereofield, electrostatic field, and hydrogen bond donor sites in the model are, respectively, 31.7%, 38.7%, and 29.6%. In the Topomer CoMFA model, the obtained q^2 is 0.674, the best number of principal components is 6, r^2 is 0.946, and the SEE is 0.193. In the CoMFA-SE model of MDA-MB-435, the resulting q^2 is 0.719, the best number of principal components is 10, r^2 is 0.991, the SEE is 0.099, and the proportions of the electrostatic field and the stereoscopic field in the model are, respectively, at 23.8% and 76.2%, it can be seen that the stereoscopic field has a greater impact on the model, In the CoMSIA-SEH model, the resulting q^2 is 0.772, the best number of principal components is 10, r^2 is 0.991, the SEE is 0.124, and the ratio of stereoscopic, electrostatic, and hydrophobic sites in the model is 24.6%, 32.3%, and 43.0%, respectively. In the Topomer CoMFA model, the resulting q^2 was 0.683, the best number of principal components was 7, r^2 was 0.959, and the SEE was 0.199.

MDA-MB-231 QSAR model analysis

When the model $q^2 > 0.5$, $r^2 > 0.9$ indicates that the model has better prediction ability, the r^2 of CoMFA-SE, CoMSIA-SED, and Topomer CoMFA of MDA-MB-231 are

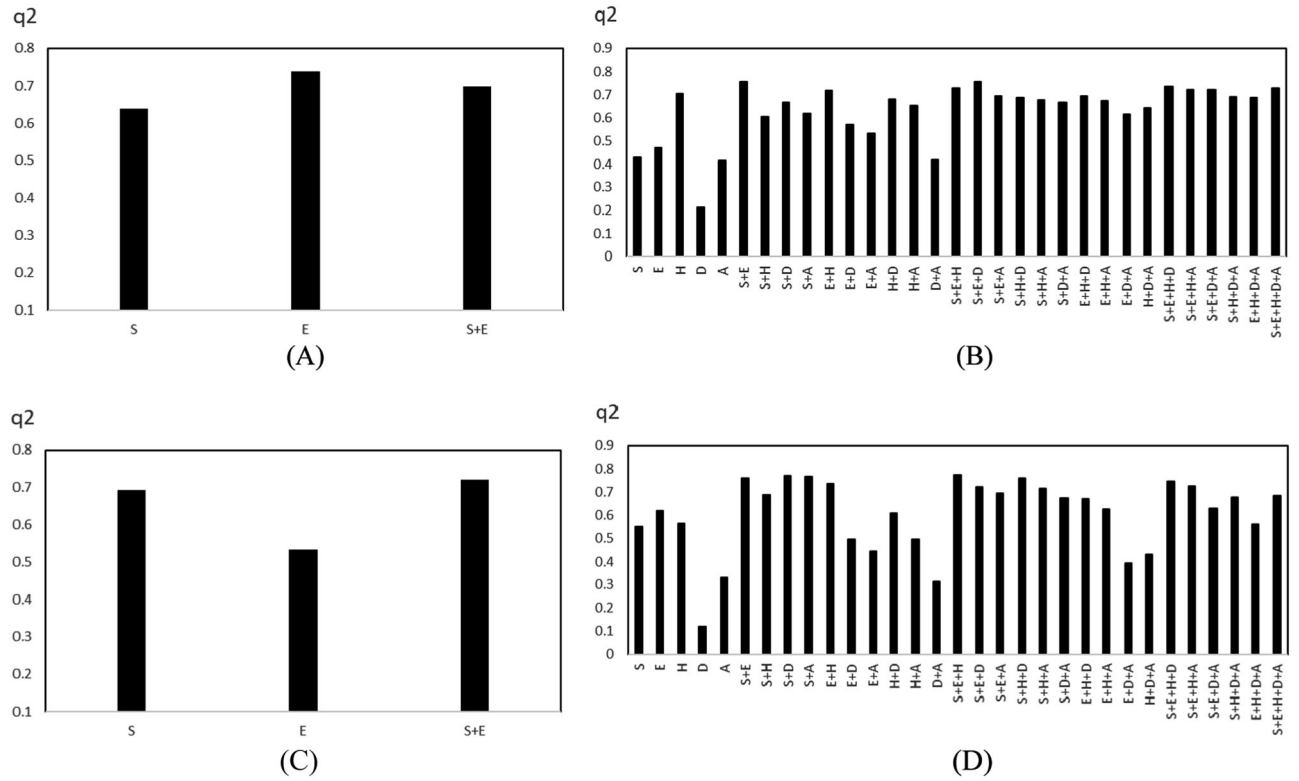

Fig. 4 **a** q^2 value of CoMFA of MDA-MB-231 model; **b** q^2 value of CoMSIA of MDA-MB-231 model; **c** q^2 value of CoMFA of MDA-MB-435 model; **d** q^2 value of CoMSIA of MDA-MB-435 model

0.994, 0.993, and 0.946, respectively. The linear regression analysis of CoMFA, CoMSIA, and Topomer CoMFA of the test set is shown in Fig. 5a–c, As can be seen from the figure, almost all compounds are located near or close to the trend line, indicating that the actual pIC50 of the compound and the predicted pIC50 have a good fit. The results show that the 3D-QSAR model is stable and has good predictions.

In the MDA-MB-231 model, the most-active No. 43 compound was used as a sample for the analysis of the three-dimensional equipotential map. Figure 6a, b is the stereoscopic field electrostatic field equipotential map of the CoMFA-SE model. In the stereoscopic field, the green area indicates that the activity of the compound increases with the increase of the group, whereas the yellow area is the opposite. As shown in the figure, there is a green equipotential region on the toluene attached to the amide group and at the Ar region, indicating that larger groups should be introduced to enhance the activity of the compound, whereas there is a larger yellow equipotential region at R1, indicating that reducing the group here will increase the activity of the compound. In the electrostatic field, the red equipotential region indicates that it is advantageous to increase the negatively charged group, the blue color indicates that the positively charged group is conducive to activity, and the CoMFA result indicates that the stereoscopic field is stronger, therefore, this model does not need to consider the introduction of electrostatic field groups to enhance compound activity. Figure 6c–e shows the stereoscopic, electrostatic, and hydrogen bond donor fields of the CoMSIA-SED model. In the hydrogen bond donor field, the blue–green indicates that increasing the hydrogen bond donor favors activity, and the purple indicates that increasing the hydrogen bond donor is detrimental to activity. As shown in the figure, in the stereoscopic field, the methyl group on the toluene attached to the amide group and the trifluoromethyl group of the Ar group have the green equipotential region, so introducing a large group here will enhance the activity of the compound. There is a yellow equipotential region at the hydroxyl group of R1, indicating that there should not be a large group here, otherwise it will reduce the activity of the compound. In the electrostatic field, the trifluoromethyl group of the Ar group, the 4th group of the benzene ring, and the 2nd and the 6th group on the toluene linked to the amide group have red equipotential region, It is explained that the introduction of negative groups here favors the activity of the compounds. There is a blue equipotential domain at the hydroxyl group of R1, so introducing a positive group here favors the

Table 2 Training set parameters for COMFA,COMSIA, and T-CoMFA models

CoMSIA	LOO		PLS			Normalized coefficients				
	np	q^2	r^2	*SEE*	*F*	*S*	*E*	*H*	*D*	*A*
A: MDA-MB-231										
S	2	0.428	0.648	0.461	27.575	1.000				
E	4	0.471	0.861	0.300	43.273		1.000			
H	10	0.704	0.982	0.121	120.797			1.000		
D	4	0.214	0.589	0.515	10.031				1.000	
A	8	0.415	0.837	0.350	15.435					1.000
S+E	10	0.755	0.993	0.077	301.473	0.423	0.577			
S+H	8	0.607	0.961	0.170	74.863	0.307		0.693		
S+D	10	0.665	0.969	0.159	69.150	0.540			0.460	
S+A	10	0.619	0.962	0.176	56.278	0.527				0.473
E+H	10	0.719	0.995	0.067	403.683		0.398	0.602		
E+D	9	0.573	0.961	0.176	62.233		0.626		0.374	
E+A	8	0.534	0.939	0.214	46.187		0.550			0.450
H+D	10	0.679	0.983	0.120	124.272			0.695	0.305	
H+A	10	0.653	0.978	0.133	99.369			0.669		0.331
D+A	10	0.417	0.905	0.279	20.997				0.394	0.606
SE+H	10	0.729	0.995	0.065	420.282	0.241	0.332	0.454		
S+E+D	10	0.755	0.993	0.076	310.021	0.317	0.387		0.296	
S+E+A	10	0.695	0.987	0.104	165.607	0.326	0.348			0.326
S+H+D	9	0.688	0.982	0.118	140.457	0.248		0.470	0.282	
S+H+A	10	0.675	0.985	0.109	149.429	0.241		0.472		0.288
S+D+A	9	0.665	0.957	0.187	49.464	0.335			0.287	0.378
E+H+D	10	0.695	0.992	0.081	273.874		0.320	0.450	0.230	
E+H+A	10	0.673	0.990	0.092	210.775		0.272	0.466		0.261
E+D+A	10	0.616	0.967	0.165	64.064		0.401		0.237	0.361
H+D+A	10	0.641	0.972	0.152	75.883			0.501	0.208	0.291
S+E+H+D	10	0.737	0.993	0.075	315.142	0.186	0.257	0.337	0.219	
S+E+H+A	10	0.721	0.992	0.079	290.538	0.187	0.218	0.352		0.243
S+E+D+A	10	0.720	0.987	0.105	162.600	0.240	0.288		0.203	0.269
S+H+D+A	10	0.691	0.983	0.120	123.671	0.201		0.376	0.108	0.244
E+H+D+A	10	0.686	0.987	0.104	165.287		0.147	0.360	0.169	0.223
S+E+H+D+A	10	0.73	0.991	0.088	229.707	0.161	0.198	0.284	0.153	0.204
CoMFA	*np*	q^2	r^2	*SEE*	*F*	*S*	*E*			
S	5	0.637	0.945	0.192	92.873	1.000				
E	10	0.74	0.972	0.153	75.235		1.000			
S+E	9	0.698	0.994	0.067	447.903	0.752	0.248			
T-CoMFA	*np*	q^2	r^2	*SEE*	*F*					
	6	0.674	0.946	0.193	76.591					
B:MDA-MB-435										
S	6	0.552	0.887	0.324	32.710	1.000				
E	7	0.620	0.943	0.236	56.228		1.000			
H	6	0.564	0.916	0.279	45.546			1.000		
D	2	0.117	0.375	0.707	8.707				1.000	
A	3	0.332	0.585	0.587	13.135					1.000
S+E	8	0.759	0.976	0.155	118.540	0.450	0.550			
S+H	9	0.687	0.980	0.144	121.197	0.341		0.659		

Table 2 (continued)

CoMSIA	LOO		PLS			Normalized coefficients				
	np	q^2	r^2	*SEE*	*F*	*S*	*E*	*H*	*D*	*A*
S+D	10	0.771	0.981	0.144	109.373	0.594			0.406	
S+A	10	0.767	0.972	0.176	72.561	0.569				0.431
E+H	10	0.735	0.985	0.128	139.492		0.414	0.586		
E+D	9	0.496	0.936	0.260	35.778		0.680		0.320	
E+A	7	0.445	0.888	0.329	27.259		0.558			0.442
H+D	10	0.609	0.968	0.187	64.468			0.737	0.263	
H+A	6	0.496	0.878	0.336	30.119			0.611		0.389
D+A	3	0.313	0.600	0.576	13.988				0.325	0.675
S+E+H	10	0.772	0.986	0.124	149.484	0.246	0.323	0.430		
S+E+D	9	0.721	0.980	0.144	122.178	0.372	0.361		0.268	
S+E+A	10	0.695	0.979	0.151	98.952	0.377	0.335			0.287
S+H+D	10	0.76	0.983	0.137	121.311	0.318		0.452	0.230	
S+H+A	10	0.715	0.980	0.148	103.285	0.313		0.444		0.242
S+D+A	9	0.674	0.965	0.191	68.335	0.488			0.183	0.329
E+H+D	10	0.668	0.985	0.130	134.169		0.324	0.481	0.185	
E+H+A	10	0.627	0.983	0.139	117.924		0.303	0.467		0.230
E+D+A	3	0.395	0.689	0.507	20.708		0.307		0.235	0.458
H+D+A	10	0.432	0.955	0.222	44.949			0.574	0.174	0.252
S+E+H+D	10	0.747	0.986	0.122	153.029	0.232	0.256	0.336	0.176	
S+E+H+A	10	0.725	0.985	0.128	139.887	0.230	0.229	0.336		0.205
S+E+D+A	10	0.632	0.981	0.144	190.753	0.318	0.276		0.180	0.225
S+H+D+A	10	0.676	0.977	0.160	88.958	0.278		0.375	0.144	0.202
E+H+D+A	10	0.562	0.982	0.140	116.057		0.270	0.406	0.131	0.193
S+E+H+D+A	10	0.684	0.985	0.130	135.355	0.211	0.203	0.289	0.120	0.174
CoMFA	*np*	q^2	r^2	*SEE*	*F*	*S*	*E*			
S	9	0.692	0.986	0.123	167.789	1.000				
E	6	0.534	0.902	0.302	38.288		1.000			
S+E	10	0.719	0.991	0.099	234.961	0.762	0.238			
T-CoMFA	*np*	q^2	r^2	*SEE*	*F*					
	7	0.683	0.959	0.199	80.137					

activity of the compound. In the hydrogen bond acceptor field, the amide bond, the 6th position on the toluene linked to the amide bond, and the amino group of the nitrogen-containing 6-membered heterocyclic ring have blue–green equipotential domain. It is explained that introducing a hydrogen bond donor here favors activity, there is a purple equipotential region at the methyl group on the toluene attached to the amide bond, therefore, hydrogen bonding donors should not be introduced here. Figure 6f–i shows the stereoscopic field, electrostatic field of R', stereoscopic field, and electrostatic field of R" in the Topomer CoMFA model. As shown in the figure, in the stereoscopic field of the R' group, there is a green equipotential region at the sixth position of the left benzene ring and at the trifluoromethyl of the right benzene ring, hence introducing large groups here will increase the activity of the compound. There is a yellow equipotential region at the fourth position of the right benzene ring, indicating that large groups should not be introduced here. In the electrostatic field of the R' group, the introduction of a negatively charged group around the left phenyl ring and the trifluoromethyl group of the right phenyl ring enhances the activity of the compound. Introduction of a positively charged group at the junction of the amide group with the right phenyl ring enhances the activity of the compound. In the stereoscopic field of the R" group, there is a yellow equipotential region at the hydroxyl group of R1, so it is not appropriate to introduce a large group here. However, the introduction of large groups near the third position of R1 increases the activity of the compound because there is a

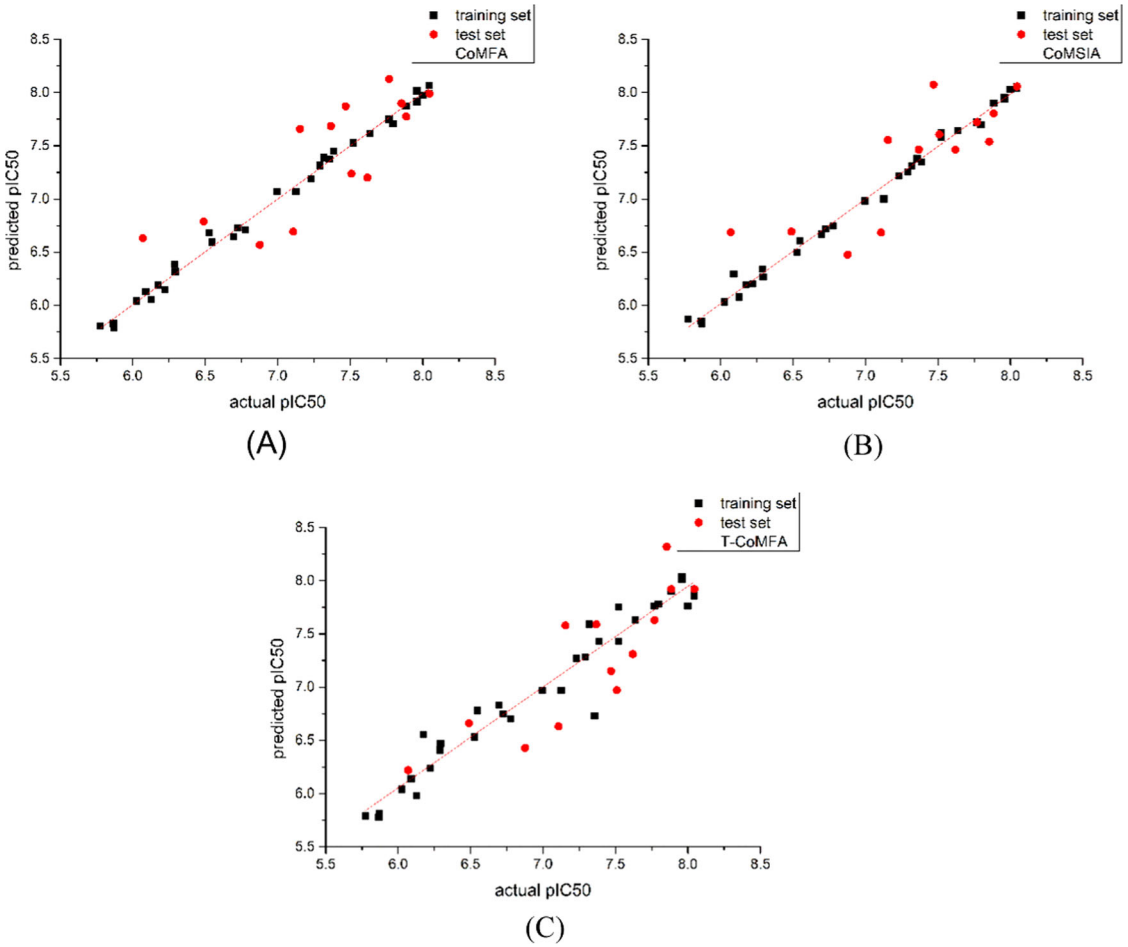

Fig. 5 Correlation between training set and test set actual value data and predicted value data. **a** COMFA model results, **b** COMSIA model results, **c** T-CoMFA model results

green equipotential region. In the electrostatic field of the R' group, as the figure shows, there is a red equipotential domain around the hydroxyl group of the R1 group, therefore, introducing negatively charged groups here will enhance the activity of the compounds. There is a blue equipotential region near the third position of the R1 group, hence introducing a positively charged group here will enhance compound activity.

MDA-MB-435 QSAR model analysis

The r^2 of CoMFA, CoMSIA, and Topomer CoMFA for MDA-MB-435 were 0.991, 0.986, and 0.959, respectively. The linear regression analysis of CoMFA, CoMSIA, and Topomer CoMFA for the training set and test set of the model is shown in Fig. 7a–c, As can be seen from the figure, almost all compounds are located near or close to the trend line, indicating that the actual pIC50 of the compound and the predicted pIC50 have a good fit. The results show that the 3D-QSAR model is stable and has good predictions.

Similarly, in the MDA-MB-435 model, the most-active No. 43 compound was used as a sample for the analysis of the three-dimensional equipotential map. Figure 8a, b shows the stereoscopic and electrostatic field equipotential map of the CoMFA-SE model. In the stereoscopic field, as shown in the figure, there is a green equipotential region at the trifluoromethyl group of the Ar group. Introducing a large group here will enhance the activity of the compound. As the results of the 3D-QSAR show that the contribution of the stereoscopic field accounts for the majority, the effects of the electrostatic field need not be over-considered. Figure 8c–e shows the stereoscopic, electrostatic, and hydrophobic fields of the CoMSIA-SEH model. In the hydrophobic field, yellow indicates that increasing the hydrophobic group is beneficial to increase activity, and white indicates that increasing the hydrophilic group favors activity. As shown in the figure, in the stereoscopic field, the hydroxyl at Ar has a green equipotential region, indicating that the introduction of a large group here favors the activity of the compound. In the electrostatic field, there is a

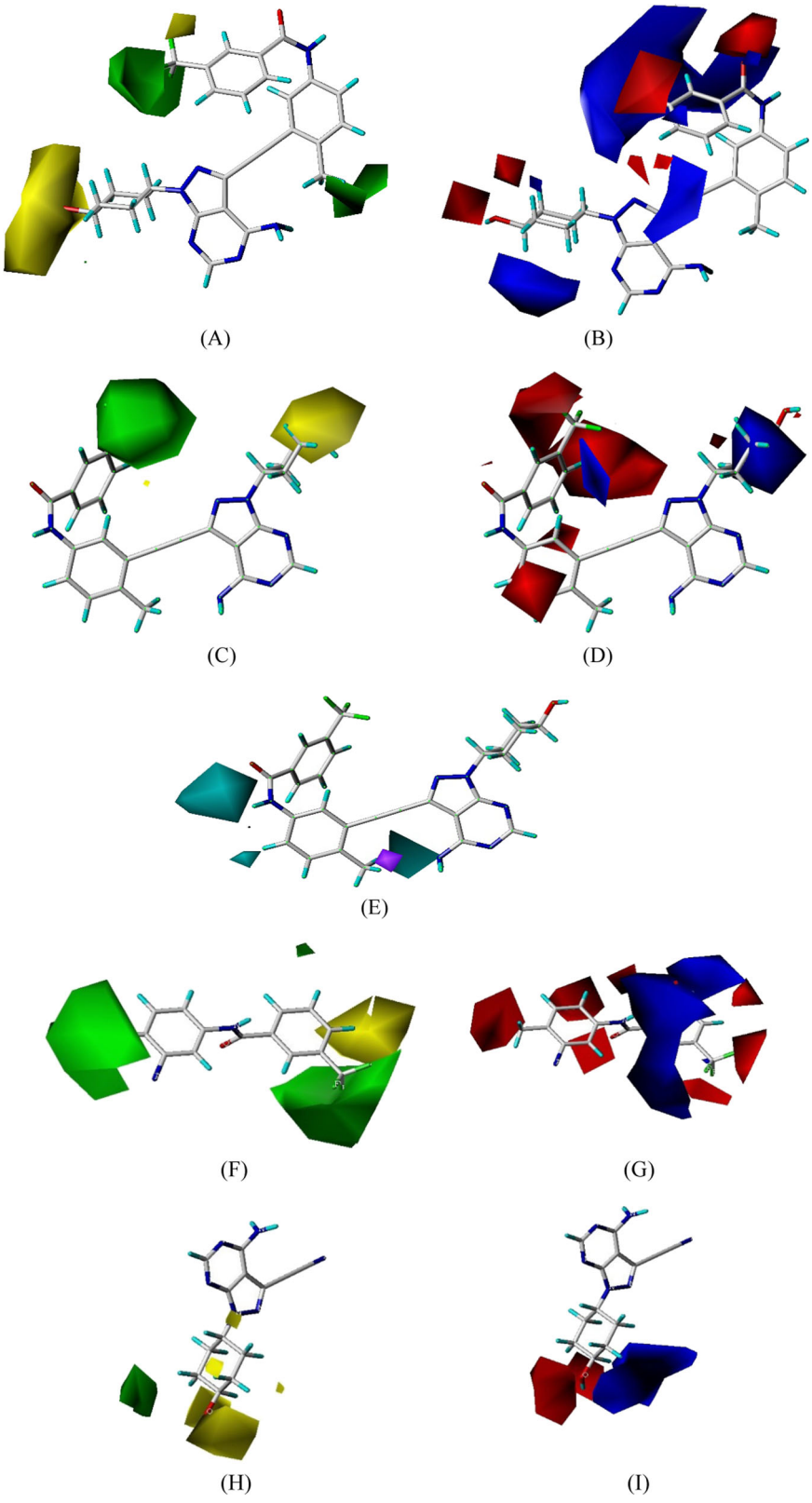

Fig. 6 Three-dimensional equipotential map of CoMFA, CoMSIA, T-CoMFA of MDA-MB-231. **a** CoMFA stereoscopic field; **b** CoMFA electrostatic field; **c** CoMSIA stereoscopic field; **d** CoMSIA electrostatic field; **e** CoMSIA hydrogen bond donor field; **f** T-CoMFA R' stereoscopic field; **g** T-CoMFA R' Electrostatic field; **h** T-CoMFA R" stereoscopic field; **i** T-CoMFA R" electrostatic field

red equipotential region at the trifluoromethyl group of Ar and the hydroxyl group of R1, indicating that a negative charge group should be introduced here. In the fourth position of Ar and the second and third positions of R1 Cyclohexyl, there is a blue equipotential region, so the introduction of positive groups here will enhance the

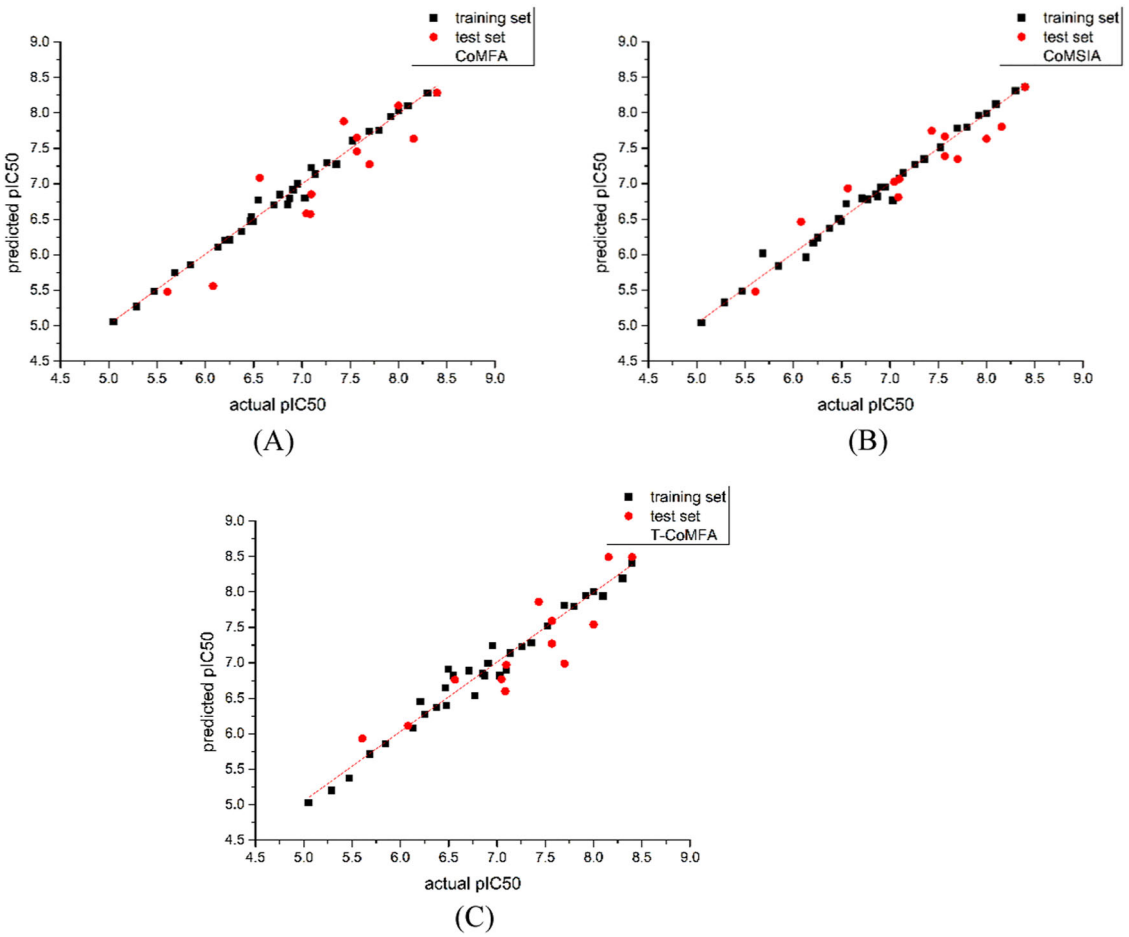

Fig. 7 Correlation between training set and test set actual value data and predicted value data. **a** COMFA model results, **b** COMSIA model results, **c** T-CoMFA model results

activity of the compound. In the hydrophobic field, there is a white equipotential region at the 5th and 6th position of the benzene ring at Ar, the methyl group of toluene connected with the amide group, and the hydroxyl group of R1, indicating that a hydrophilic group should be introduced here. There is a yellow equipotential region at the 4th position of the benzene ring at Ar, a trifluoromethyl group, and at the 5th and 6th positions of cyclohexyl at R1. Therefore, introduction of a hydrophobic group here facilitates the increase of the activity of the compound. Figure 8f–i shows the stereoscopic field, electrostatic field of R', stereoscopic field, and electrostatic field of R" in the Topomer CoMFA model. In the stereoscopic field of the R' group, as shown in the figure, the trifluoromethyl group at Ar and the fourth position have a green equipotential region, Although there is also a yellow equipotential region at the fourth position, it is farther away, so introducing large groups here will increase the activity of the compound. In the electrostatic field of the R' group, as shown in the figure, there is a red equipotential region around the methyl group of the upper benzene ring and the trifluoromethyl group at Ar, hence the introduction of negatively charged groups here will enhance the activity of the compounds, There is a blue equipotential region at the four-sixth position at Ar, so introducing a positively charged group here will enhance compound activity. In the stereoscopic field of the R" group, as shown in the figure, there is a yellow equipotential region at the hydroxyl group at R1, so it is not appropriate to introduce a large group here, there is a green equipotential region near the fifth position at R1, so introducing large groups here can increase the activity of the compound. In the electrostatic field of the R" group, as shown in the figure, there is a red equipotential region at the third position of the R1 group and at the hydroxyl group. Therefore, introduction of a negatively charged group here enhances the activity of the compound. The third position of the R1 group also has a blue equipotential region, but is farther away than the red equipotential region, so positively charged groups should not be introduced.

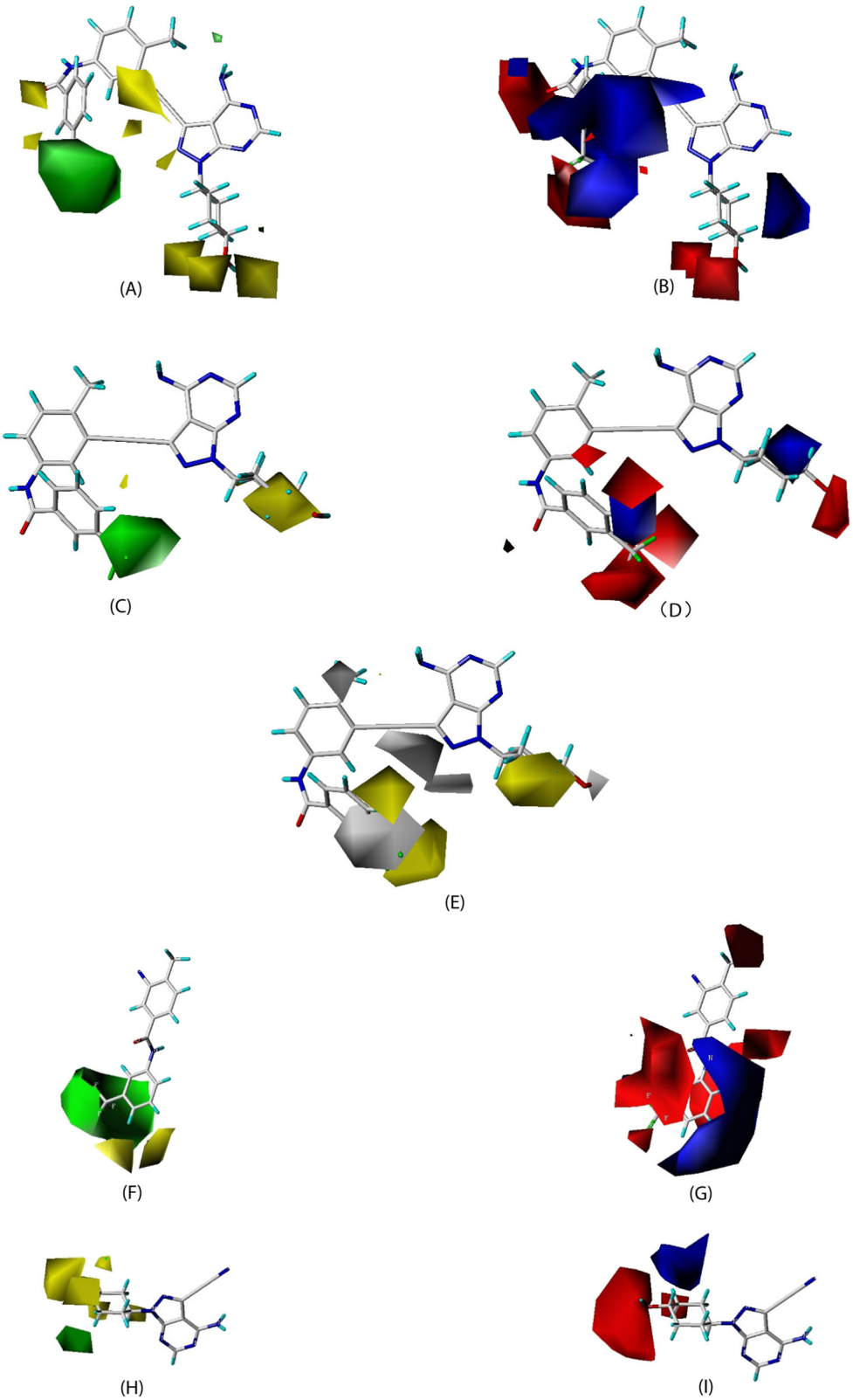

Fig. 8 Three-dimensional equipotential map of CoMFA, CoMSIA, T-CoMFA of MDA-MB-231. **a** CoMFA stereoscopic field; **b** CoMFA electrostatic field; **c** CoMSIA stereoscopic field; **d** CoMSIA electrostatic field; **e** CoMSIA hydrogen bond donor field; **f** T-CoMFA R' stereoscopic field; **g** T-CoMFA R' Electrostatic field; **h** T-CoMFA R" stereoscopic field; **i** T-CoMFA R" electrostatic field

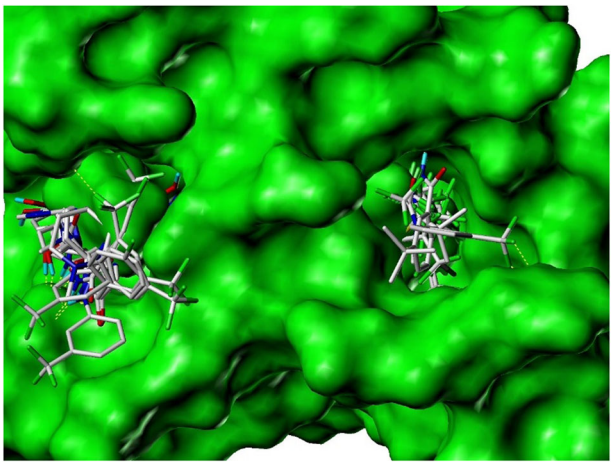

Fig. 9 The docking conformation of Src protein with all compounds

Molecular docking results and analysis

Molecular docking combines multiple drug design methods to dock between the ligand and the receptor. The 51 molecules were molecularly docked with the crystal structure of Src (PDB:3E7L). After setting the docking bag with Surflex-Dock, specify the ligand to be docked. Figure 9 shows the docking superposition map of 51 small molecule compounds and Src protein receptors. From the analysis in the figure, the compounds are all well-superimposed in the active pocket of the receptor, and the small molecule compound binds closely to the receptor. This laid a structural basis for the inhibition of the Src receptor by such small molecule compounds. The obtained compound No. 21 molecule was scored as high as 12.8775. Figure 10a shows the dock of No. 21 molecule with the acceptor. It can be seen that there are two hydrogen bonds connected to it

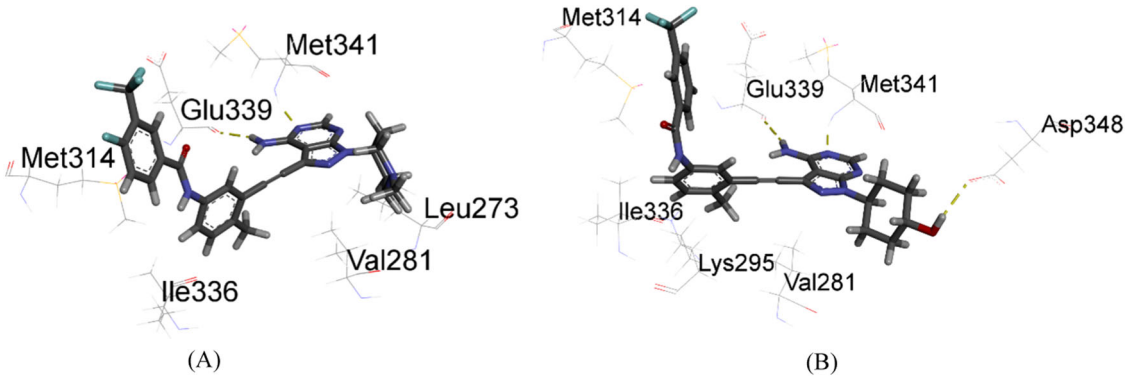

Fig. 10 The three-dimensional diagram of the molecular docking. **a** The docking interactive model of Src protein receptor with compound 21. **b** The docking interactive model of Src protein receptor with compound 43 (the yellow dotted line represents the hydrogen bond)

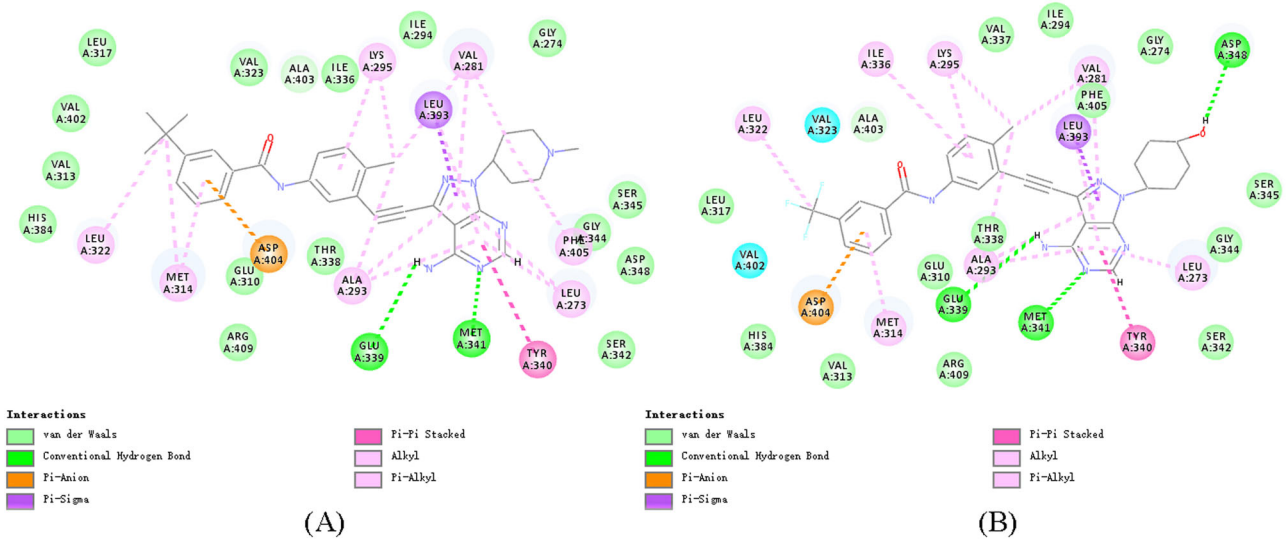

Fig. 11 The two-dimensional diagram of the molecular docking. **a** The docking interactive model of Src protein receptor with compound 21. **b** The docking interactive model of Src protein receptor with compound 43

Table 3 The new compounds of structure and predicted activity

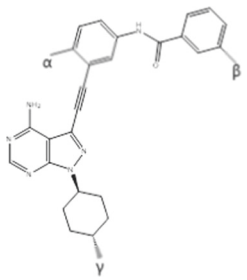

MDA-MB-231：

NO.	α	β	γ	CoMFA	CoMSIA	T-CoMFA	Docking score
A	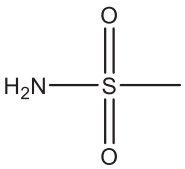	NH_2	NO_2	7.860	7.965	7.81	11.7417
B	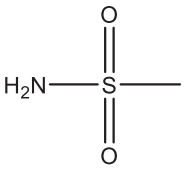	NH_2	CN	7.911	7.954	7.80	8.6568
C	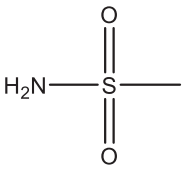	NH_2	CHO	7.884	7.939	7.73	7.1380
D	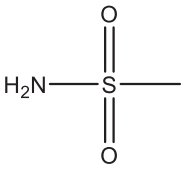	OH	NO_2	8.229	7.927	7.89	10.9414
E	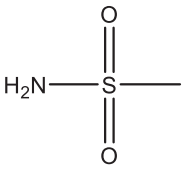	OH	CN	8.182	7.964	7.93	7.2606
F	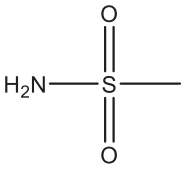	OH	CHO	8.150	8.030	7.99	8.6375
G	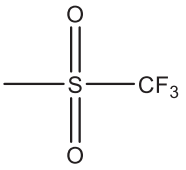	NH_2	CN	7.719	7.867	7.88	9.7023

Table 3 (continued)

NO.	α	β	γ	CoMFA	CoMSIA	T-CoMFA	Docking score
H	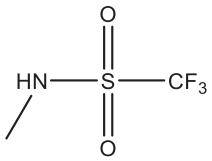	NH_2	NO_2	7.981	7.815	7.81	9.7983
I	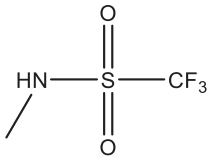	NH_2	CN	7.975	7.879	7.92	9.9060
J	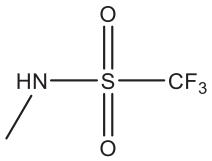	NH_2	CHO	7.951	7.819	7.89	8.8516
K	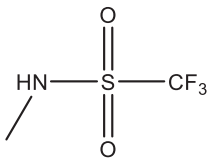	OH	NO_2	8.228	7.954	7.91	8.9130
L	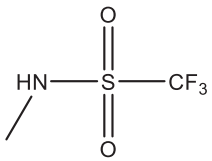	OH	CN	8.137	7.990	8.06	9.9881
M	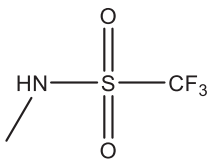	OH	CHO	8.159	8.023	8.13	8.2680

MDA-MB-435 :

NO.	α	β	γ	CoMFA	CoMSIA	T-CoMFA	Docking score
a	NH_2	CF_3	NH_2	8.291	8.223	8.41	8.5478
b	NH_2	CF_3	OH	8.398	8.379	8.32	7.8354
c	OH	CF_3	OH	8.132	8.179	8.42	9.3217
d	CHO	CF_3	NH_2	8.208	8.216	8.21	9.2247
e	CHO	CF_3	OH	8.161	8.191	8.52	7.9983
f	NH_2	CCl_3	OH	8.292	8.198	8.60	10.0092
g	NH_2	CCl_3	COOH	8.246	8.376	8.58	8.2354
h	OH	CCl_3	COOH	8.238	8.267	8.43	9.3157
i	NH_2	CBr_3	OH	8.427	8.167	8.57	8.1572
j	NH_2	CBr_3	COOH	8.263	8.413	8.59	9.3517
k	OH	CBr_3	COOH	8.199	8.277	8.43	8.2175

and they are indicated by yellow dashed lines. The hydrogen atom on the amino group on the six-membered ring of the ligand forms a hydrogen bond through the negative charge and an oxygen atom on the side chain of the GLU339 of the acceptor, The hydrophilic pocket formed by the pocket between the ligand and the target protein can be seen on the same side. The nitrogen atom in the third position of this six-membered ring forms a hydrogen bond through the hydrophobic and hydrogen atoms on the side chain of the acceptor MET341. After the most-active molecule No. 43 was docked with the receptor, the connected hydrogen bonds shown in Fig. 10b were indicated by yellow dashed lines. It can be seen that the small molecule ligand No. 43 and the No. 21 molecule form two hydrogen bond ligands at the same position. But the hydrogen atom on the phenolic hydroxyl group on the R1 group of the No. 43 molecule forms a hydrogen bond through the negative charge and the oxygen atom on the side chain of the acceptor ASP348. From this point of view, the No. 43 molecule is more closely linked to the target, because the formation of hydrogen bonds makes the binding between the ligand and the receptor more tight, and the No. 43 molecule forms three hydrogen bonds with the receptor. No. 21 molecules only form two hydrogen bonds with the receptor, so the No. 43 molecule can form a stronger inhibitory effect on the receptor protein. The two-dimensional docking diagram is shown in Fig. 11a, b, and the effect of amino acids on it can be seen more clearly.

New compound design and activity prediction

Based on the established two sets of 3D-QSAR models and related analysis results, the No. 43 compound was used as a template to modify its molecular structure. According to the 3D-QSAR model of MDA-MB-231, 13 new compounds were designed. According to the 3D-QSAR model of MDA-MB-435, 11 new compounds were designed. The structure of the new compounds is shown in Table 3.

A molecular docking analysis of the new compounds showed that all the new compounds had the same docking pattern as the No. 43 compound. On the basis of ligand superposition, the activity prediction was performed using the established 3D-QSAR model, and the predicted activity values of the obtained 3D-QSAR model are shown in Table 3. Predictions using CoMFA, CoMSIA, or T-CoMFA models indicate that the new compounds have an inhibitory effect on Src, and the predicted PIC50 values are greater than the PIC50 values of the 48th molecule selected by Zhang et al. (2016). The molecular docking of the designed compounds was performed. The docking score results are shown in Table 3. It is explain that the design of new compounds may become new Src inhibitors.

Conclusion

In this study, 3D-QSAR models of CoMFA, CoMSIA, and Topomer CoMFA were established using Src inhibitors of 3-(phenylethynyl)-1H-pyrazolo[3,4-d]pyrimidin-4-amine derivatives. The model has a relevant statistical correlation, indicating that the model has a good predictive ability. In addition, the results of the CoMFA, CoMSIA, and Topomer CoMFA models were cross-validated by molecular docking studies. It can be seen intuitively in the docking diagram that the selected molecule and ligand pocket are highly compatible and can be used as a reference for the synthesis of drug structures. Based on CoMFA, CoMSIA, Topomer CoMFA model modeling, and molecular docking analysis, No. 21 and No. 43 molecules were proposed as the most potential. Using these two representative molecules as templates, the effects of the size, hydrophobicity, and hydrogen bond of the introduced groups at different sites on the overall activity of the molecule were analyzed, and it provides a theoretical basis for further research. At the same time, a new compound design was performed based on the model of the two cell lines, and the predicted PIC50 values all have an effective inhibitory effect on Src, this shows that the model is effective and reliable. Therefore, computer-aided drug design and molecular docking such as 3D-QSAR provide important theoretical basis for guiding the design of new highly active molecules, avoiding blindness and improving efficiency.

Acknowledgements We are grateful to the national natural science foundation of China (81171508); Key project of Chongqing natural science foundation (cstc2015jcyjBX0080); Scientific and technological research project of Chongqing municipal education commission (kjzd-k201801102, KJQN201801132); Supported by the scientific research startup fund of Chongqing university of technology (2017ZD42).

Compliance with ethical standards

Conflict of interest The authors declare that they have no conflict of interest.

References

Bianchini G, Balko JM, Mayer IA, Sanders ME, Gianni L (2016) Triple-negative breast cancer: challenges and opportunities of a heterogeneous disease. Nat Rev Clin Oncol 13(11):674–690

Bush BL, Nachbar RB (1993) Sample-distance partial least squares: pls optimized for many variables, with application to comfa. J Comput Aided Mol Des 7(5):587–619

Das J, Chen P, Norris D, Padmanabha R, Lin J, Moquin RV (2006) 2-aminothiazole as a novel kinase inhibitor template. structure? activity relationship studies toward the discovery of *n*-(2-chloro-

6-methylphenyl)-2-[[6-[4-(2-hydroxyethyl)-1-piperazinyl)]-2-methyl-4-pyrimidinyl]amino)]-1,3-thiazole-5-carboxamide (dasatinib, bms-354825) as a potent *pan*-src kinase inhibitor. J Med Chem 49(23):6819–6832

Davis SL, Eckhardt SG, Tentler JJ, Diamond JR (2014) Triple-negative breast cancer: bridging the gap from cancer genomics to predictive biomarkers. Ther Adv Med Onocl 6(3):88–100

Dent R, Trudeau M, Pritchard KI, Hanna WM, Kahn HK, Sawka CA (2007) Triple-negative breast cancer: clinical features and patterns of recurrence. Clin Cancer Res 13(15):4429–4434

Finn RS, Bengala C, Ibrahim N, Roche H, Sparano J, Strauss LC (2011) Dasatinib as a single agent in triple-negative breast cancer: results of an open-label phase 2 study. Clin Cancer Res 17 (21):6905–6913

Haltia UM, Andersson N, Yadav B (2017) Systematic drug sensitivity testing reveals synergistic growth inhibition by dasatinib or mtor inhibitors with paclitaxel in ovarian granulosa cell tumor cells. Gynecol Oncol 144(3):621–630

Kakarla P, Inupakutika M, Devireddy AR, Gunda SK, Willmon TM, Ranjana KC (2016) 3d-qsar and contour map analysis of tariquidar analogues as multidrug resistance protein-1 (mrp1) inhibitors. Int J Pharm Sci Res 7(2):554

Kim LC, Song L, Haura EB (2009) Src kinases as therapeutic targets for cancer. Nat Rev Clin Oncol 6(10):587–595

Lehmann B (2011) Identification of human triple-negative breast cancer subtypes and preclinical models for selection of targeted therapies. J Clin Invest 121(7):2750

Liedtke C, Rody A (2015) New treatment strategies for patients with triple-negative breast cancer. Curr Opin Obstet Gyn 27(1):77–84

Massard C, Mateo J, Loriot Y, Pezaro C, Albiges L, Mehra N (2017) Phase i/ii trial of cabazitaxel plus abiraterone in patients with metastatic castration-resistant prostate cancer (mcrpc) progressing after docetaxel and abiraterone. Ann Oncol 28(1):90–95

Mayer EL, Krop IE (2010) Advances in targeting src in the treatment of breast cancer and other solid malignancies. Clin Cancer Res 16 (14):3526–3532

Montero JC, Seoane S, Ocaña Alberto, Pandiella A (2011) Inhibition of src family kinases and receptor tyrosine kinases by dasatinib: possible combinations in solid tumors. Clin Cancer Res 17 (17):5546–5552

Morales-Bayuelo A, Ayazo H, Vivas-Reyes R (2010) Three-dimensional quantitative structure–activity relationship comsia/comfa and leapfrog studies on novel series of bicyclo [4.1.0] heptanes derivatives as melanin-concentrating hormone receptor r1 antagonists. Eur J Med Chem 45(10):4509–4522

Myoui A, Nishimura R, Williams PJ, Hiraga T, Tamura D, Michigami T (2003) C-src tyrosine kinase activity is associated with tumor colonization in bone and lung in an animal model of human breast cancer metastasis. Cancer Res 63(16):5028–5033

Okamoto W, Okamoto I, Yoshida T, Okamoto K, Takezawa K, Hatashita E (2010) Identification of c-src as a potential therapeutic target for gastric cancer and of met activation as a cause of resistance to c-src inhibition. Mol Cancer Ther 9(5):1188–1197

Pan Y, Zheng M, Zhong L, Yang J, Zhou S, Qin Y, Xiang R, Chen Y, Yang SY (2015) A preclinical evaluation of SKLB261, a multikinase inhibitor of EGFR/Src/VEGFR2, as a therapeutic agent against pancreatic cancer. Mol Cancer Ther 14(2):407

Park SI, Zhang J, Phillips KA, Araujo JC, Najjar AM, Volgin AY (2008) Targeting src family kinases inhibits growth and lymph node metastases of prostate cancer in an orthotopic nude mouse model. Cancer Res 68(9):3323–3333

Park SY, Kim HM, Koo JS (2015) Differential expression of cancer-associated fibroblast-related proteins according to molecular subtype and stromal histology in breast cancer. Breast Cancer Res Treat 149(3):727–741

Pathak HB, Yan Z, Geetika S, Jeff H, Schilder RJ, Golemis EA (2015) A synthetic lethality screen using a focused sirna library to identify sensitizers to dasatinib therapy for the treatment of epithelial ovarian cancer. PloS ONE 10(12):e0144126

Pichot CS, Hartig SM, Xia L, Arvanitis C, Monisvais D, Lee FY (2009) Dasatinib synergizes with doxorubicin to block growth, migration, and invasion of breast cancer cells. Br J Cancer 101 (1):38–47

Rexer BN, Arteaga CL (2012) Intrinsic and acquired resistance to her2-targeted therapies in her2 gene-amplified breast cancer: mechanisms and clinical implications. Crit Rev Oncog 17 (1):1–16

Seggewiss R, Price D, Purbhoo M (2008) Immunomodulatory effects of imatinib and second-generation tyrosine kinase inhibitors on t cells and dendritic cells: an update. Cytotherapy 10(6):633–641

Sharma R, Dhingra N, Patil S (2016) Comfa, comsia, hqsar and molecular docking analysis of ionone-based chalcone derivatives as antiprostate cancer activity. Indian J Pharm Sci 78(1):54–64

Shields BJ, Wiede F, Gurzov EN, Wee K, Hauser C, Zhu HJ (2013) Tcptp regulates sfk and stat3 signaling and is lost in triple-negative breast cancers. Mol Cell Biol 33(3):557–570

Taha MO, Habash M, Khanfar MA (2014) The use of docking-based comparative intermolecular contacts analysis to identify optimal docking conditions within glucokinase and to discover of new gk activators. J Comput Aided Mol Des 28(5):509–547

Tarpley M, Abdissa TT, Johnson GL, Scott JE (2014) Bosutinib reduces the efficacy of dasatinib in triple-negative breast cancer cell lines. Anticancer Res 34(4):1629–1635

Tryfonopoulos D, Walsh S, Collins DM, Flanagan L, Quinn C, Corkery B (2011) Src: a potential target for the treatment of triple-negative breast cancer. Ann Oncol 22(10):2234–2240

Wendt B, Cramer RD (2014) Challenging the gold standard for 3d-qsar: template comfa versus x-ray alignment. J Comput Aided Mol Des 28(8):803–824

Zhang S, Huang WC, Zhang L, Zhang C, Lowery FJ, Ding Z (2013) Src family kinases as novel therapeutic targets to treat breast cancer brain metastases. Cancer Res 73(18):5764–5774

Zhang CH et al. (2016) From lead to drug candidate: optimization of 3-(phenylethynyl)-1H-pyrazolo[3,4-d]pyrimidin-4-amine derivatives as agents for the treatment of triple negative breast cancer. J Med Chem 59(21):9788–9805

Zhang L, Tsai KC, Du L, Fang H, Li M, Xu W (2011) How to generate reliable and predictive comfa models. Curr Med Chem 18(6):923–930